Determination of the mean tunneling flight time in the Büttiker-Landauer oscillating-barrier model as the reflected phase time

Reuven Ianconescu [1,2] and Eli Pollak [1]
[1] *Chemical and Biological Physics Department, Weizmann Institute of Science, 76100, Rehovoth, Israel*
[2] *Shenkar College of Engineering and Design, Anna Frank St. 12, Ramat Gan, Israel*

(Received 25 February 2021; accepted 22 March 2021; published 20 April 2021)

The oscillating-barrier model was used by Büttiker and Landauer to determine a "traversal time for tunneling." The model sets a timescale but is not the physically measured flight time of a wave packet scattered on the oscillating-barrier potential. In this paper we show that the flight time in the limit of a narrow-in-momentum wave packet is given by the reflected phase time associated with the various branches of the scattered particle. This is but another example which establishes that tunneling flight times are a reflection of the Wigner phase times. As such, the oscillating-barrier model does not add any new information about tunneling flight times which has not been elucidated previously using static barrier models.

DOI: 10.1103/PhysRevA.103.042215

I. INTRODUCTION

Büttiker and Landauer [1] in their paper on tunneling times considered the effect of an oscillating symmetric square barrier on the tunneling dynamics to determine what they termed the "traversal time for tunneling." The timescale they elucidated is now well understood as being the so-called imaginary tunneling time [2,3] rather than the flight time through the barrier as would be measured in a time-of-flight experiment. But what then is the flight time and how is it affected by the oscillating barrier as compared with a static barrier?

Büttiker and Landauer negated the possibility that this time would be related to Wigner's phase time [4]: in their words "A time delay for a scattering process can be calculated by following the peak of a wave packet, ...the time found is $\tau_\phi = \hbar\partial\phi/\partial E$ .... There seems little physical justification, however, for the identification of incident peaks with transmitted peaks, particularly in the presence of the strong deformation of a wave packet transmitted through a barrier." Büttiker [5] repeated this thought in his now classical paper on Larmor precession times (see though a partial critique in Ref. [6]). A similar conclusion appears later in a paper by Steinberg [7] who, citing Büttiker and Landauer, states that the phase time "describes the appearance of a wave packet peak on the far side of the barrier. It has been pointed out that there is no fundamental reason in quantum theory to associate a 'delay' time of this sort with the duration of the interaction itself."

These claims were controversial. Collins, Lowe, and Barker [6], in their review of the tunneling-time problem stated explicitly that "the phase-time result originally obtained by Wigner and by Hartman [8] is the best expression to use for a wide parameter range of barriers, energies and wave-packets." Nimtz [9] further used the phase time to justify the existence of superluminal tunneling. A recent study of superluminal tunneling times within a relativistic framework may be found in Ref. [10].

In recent work, we have shown that these statements are not precise in more than one way. The tunneling wave packet is not necessarily deformed strongly [11]. If the properties of an incident Gaussian wave packet are such that particles are transmitted only via tunneling, then the incident wave packet is not deformed. The transmitted wave packet is very similar in shape to the incident one, except that its amplitude is lowered significantly due to the low transmission probability. Second, the phase time is related to the mean time of flight of the transmitted or reflected particles in the limit that the momentum variance of the incident wave packet vanishes. If, due to the Gaussian nature of the incident wave packet a steepest descent estimate is valid for its time dependence, then the mean time of flight is identical to the peak time.

The tunneling time controversy was reignited in recent years by the advent of ultrafast lasers and attosecond metrology [12,13]. Sainadh *et al.* [14] recently reported attoclock and momentum-space imaging [15] experiments on atomic hydrogen and compared these results with simulations based on the full three-dimensional time-dependent Schrödinger equation. They found good agreement between measured and simulated data, confirming the conclusions of an earlier theoretical study [16] of the attoclock technique in atomic hydrogen that presented a compelling argument for instantaneous tunneling. A different conclusion was reached by Ramos *et al.* [17] who measured the Larmor clock time and concluded that the tunneling time of Rb atoms through a Gaussian barrier is finite. This was then reconfirmed by Spierings and Steinberg with a second experiment in which the incident energy of the Rb atoms was under more precise control [18].

It is in this context that we decided to take a renewed but different look at the Büttiker-Landauer "experiment." As in our previous work [10,11,19,20], we study the transition path time of flight of an incident Gaussian wave packet which is observed at screens located sufficiently far to the right and left

of the symmetric square barrier. In principle, the time of flight is readily observable experimentally. It is well understood that the oscillating barrier causes the scattered particle to absorb or emit quanta of energy which are proportional to the frequency of the oscillation [1]. This leads respectively to a higher or lower momentum of the scattered particle. The conditions of our numerical experiment are such that the screen locations are placed sufficiently far from the barrier so that the time of arrival of each subwave packet does not interfere with that of the other. This allows us to "measure" a flight time for each subwave packet separately and compare their mean transmitted and reflected times. As in our previous studies, we choose an incident wave packet (from the left) whose incident energy is below the barrier height and whose momentum width is sufficiently narrow to assure that above-barrier transmission is negligible even when the particle absorbs energy from the field and that initially there is no significant leakage into the region to the right of the barrier.

In addition to the momentum-filtering effect [21] which exists for the static barrier, the field accelerates or slows down the incident particles. It is thus a challenge to separate these in a sense trivial effects of the barrier from the tunneling time itself. This is answered by using two different strategies: First, we compare the mean transmitted and reflected flight times of each class of subpackets separately; that is, the mean times of the subpacket with one absorbed quantum are compared with each other, and similarly for those with one quantum emitted and the elastic ones. As in our previous studies [11,19,20] we find that, in the limit that the momentum width of the incident wave packet vanishes, so that momentum filtering is negligible, the mean times of the "elastic" (no net transfer of quanta to or from the particle) transmitted and reflected subpackets are almost identical. This is not the case for the sub bands with one emitted or absorbed quantum. In these cases, in the limit of zero momentum width, the transmitted particle is delayed by the oscillating barrier as compared with the reflected particle. This delay is precisely as predicted by the phase time for the respective subpackets, indicating that the phase time is the correct measure for the effect of the interaction on the flight time of the particle.

To determine the actual tunneling time it is necessary to study the mean transmitted time by itself, rather than by a comparison with the mean reflected time. This poses a difficulty. The mean transmission time is comprised of motion outside the barrier region and inside the barrier region. When considering peaks, one could compare the peak arrival time in the presence of the oscillating barrier and in its absence. However, the mean flight time of a free particle diverges due to the t^{-1} long time tail of the density. To overcome this difficulty we compare the mean transmission time in the presence of the oscillating barrier with the mean transmission time in the absence of the barrier but in the presence of the same localized field. We find that, in the limit of vanishing width, the mean time difference between scattering in the presence of the oscillating field but once with the barrier and once without it, not only does not vanish but is given with good accuracy by the phase time at the energy of the subpacket. It is not related to the Büttiker-Landauer traversal time, which is the imaginary time [3]. The tunneling flight time, with an oscillating barrier or without it is given by the phase time at the respective energy. Our conclusion then is that the Büttiker-Landauer experiment provides perhaps interesting information on the potential but does not provide new information on tunneling flight times which is not known from scattering on a static barrier.

In Sec. II we describe the Büttiker-Landauer setup, the incident wave packet, field strength, and other relevant parameters needed to formulate the scattering process and the flight-time distributions. Numerical wave-packet propagation results are then presented in Sec. III. We end with a discussion stressing that although the Büttiker-Landauer experiment as originally defined does not reveal the tunneling flight time, it does show a route for the experimental determination of the imaginary tunneling time, a task which is not less difficult than observing flight times.

II. CONFIGURATION AND FORMULATION

The theory for the Büttiker-Landauer transmission and reflection coefficients is reviewed briefly in Appendix A and the theory for the phase times in Appendix B. The parameters used in this paper are described in Table I in atomic units.

The oscillating-barrier potential is taken to be

$$V(x,t) = [V_0 + V_1 \sin(\omega t)]\mathrm{rect}\left(\frac{x}{2a}\right), \tag{1}$$

where rect is the rectangular function, so that the barrier is centered at $x = 0$, its width is $2a$, the time-independent barrier height is V_0 and the oscillation amplitude of the barrier is V_1, see Table I. The incident particle is described by the coherent-state wave function

$$\Psi_i \equiv \Psi(x, t = 0) = \left[\frac{\Gamma}{\pi}\right]^{1/4} \exp\left[-\frac{\Gamma}{2}(x - x_0)^2 + ip_0 x/\hbar\right], \tag{2}$$

where x_0 is the central position of the initial wave packet, located to the "left" of the barrier, p_0 is the positive mean initial momentum chosen so that the kinetic energy E_0 is 50% of the barrier height V_0, i.e.,

$$E_0 = \frac{p_0^2}{2M} = \frac{V_0}{2}, \tag{3}$$

and $\hbar^2\Gamma$ is twice the momentum variance of the wave packet, and its value in the numerical implementation will be scaled according to $\hbar^2\Gamma_0$ (see Table I). The wave number inside the barrier is defined as

$$\kappa = \sqrt{2M(V_0 - E_0)}/\hbar, \tag{4}$$

and the transmission probability through the static barrier is roughly $\exp(-2\kappa a)$. The incident wave packet is chosen with parameters which assure that the probability of initially finding the particle in the vicinity of the barrier $[\exp(-\Gamma x_0^2)]$ is negligible. Similarly, the momentum variance of the initial wave packet is chosen to be sufficiently small to assure that any above-barrier scattering is negligible, implying the condition

$$\frac{[p_0 + \sqrt{\hbar^2\Gamma_0}]^2}{2M} \ll V_0. \tag{5}$$

TABLE I. List of parameters.

$\hbar$	1	Reduced Planck constant
V_0	0.008	Basic barrier height
V_1	$V_0/100$	Oscillation amplitude of barrier
ω	$V_0/4\hbar$	Angular frequency of oscillating barrier
a	20	Half barrier width
$\hbar^2\Gamma_0$	4.041×10^{-6}	Twice momentum variance of incident wave packet
x_0	-3644	Central position of the initial wave packet
p_0	0.0894	Central momentum of the initial wave packet
M	1	Mass of particle
x	[−145 760 145 760]	Solution domain in space, step 1
t	[0 855 568]	Solution domain in time, step 0.25

As may be seen from inspection of Table I both conditions are satisfied by the parameters chosen. The typical initial wave packet employed (using Γ_0) and the static barrier are shown in Fig. 1. The initial wave packet is propagated in time by solving the one-dimensional (1D) time-dependent Schrödinger equation, using the split operator Fourier method [22] with a time step $dt = \hbar/(500V_0)$ over the space solution domain—see Table I.

As shown in Ref. [1], the barrier oscillating at angular frequency ω has the effect of adding sideband wave packets with energies

$$E_n = E_0 + n\hbar\omega, \tag{6}$$

where E_0 is defined in (3) and n is any integer for which $E_n > 0$ is satisfied. The parameters we use allow us to detect the lower-energy sideband $n = -1$. We will analyze the main wave packet of energy E_0 and the two sidebands $n = \pm 1$. The central momenta for these wave packets are p_0 (main) and $p_\pm = (p_0^2 \pm 2M\hbar\omega)^{1/2}$ for the sidebands. The density in the momentum domain $|\Psi(p)|^2$ after the interaction with the barrier is over, at time $t = 91\,671$, is shown in Fig. 2 on a logarithmic scale. The peaks of the wave packets are higher by around ten orders of magnitude relative to the minima, showing a good separation between them.

The momentum density of the scattered wave packets may be approximated within a steepest descent approximation as

$$|\Psi_n(p)|^2 = |X_n(p)p_n/p_0|^2 \frac{1}{\sqrt{\pi\hbar^2\Gamma}} \times \exp\left(-\frac{\left(\sqrt{p^2 - 2M\hbar\omega n} - p_0\right)^2}{\hbar^2\Gamma}\right), \tag{7}$$

where n is the sideband number, X is either D (A9) or A (A10) as defined in Appendix A. Inspection of Fig. 2 shows quantitative agreement between the numerical exact result (blue solid line) in Fig. 2 and the steepest descent approximation of Eq. (7).

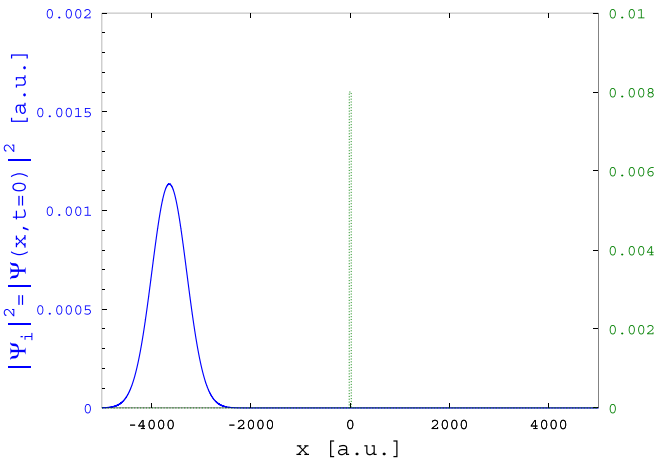

FIG. 1. The incident density $|\Psi_i|^2$ (solid blue line) and the static part of the potential V_0 (dotted green line) are plotted as functions of the particle coordinate. Note the large spatial width of the incident density, which is necessary to assure no momentum leakage above the barrier. On this scale, the width of the barrier is rather small.

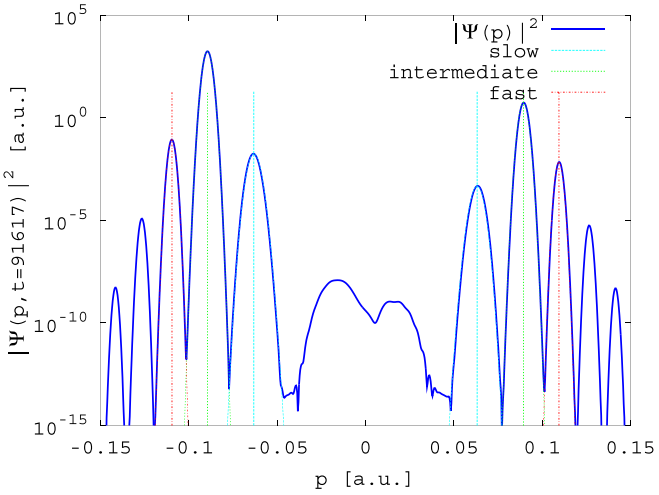

FIG. 2. The momentum density $|\Psi(p)|^2$ (solid blue line) after the interaction with the barrier is over ($t = 91\,671$) is plotted on a logarithmic scale vs the final momentum. Positive (negative) momenta imply transmission (reflection) of the incident wave packet. The vertical (dashed cyan, dotted green, dash-dotted red) lines denote the momenta p_-, p_0, and p_+, respectively, and are referred to as slow, intermediate, and fast. The steepest descent approximations to the momentum density given in Eq. (7) are shown on the same plot, using the same colors and line styles for the slow, intermediate, and fast wave packets. Note how well the steepest descent estimates agree with the numerically exact results.

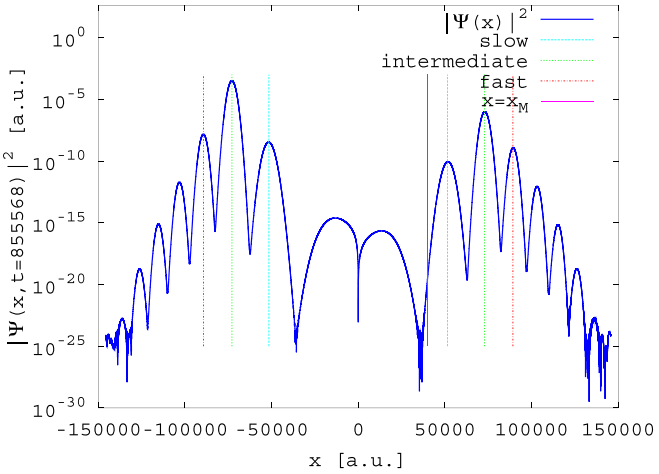

FIG. 3. The numerically evolved spatial density $|\Psi(x)|^2$ (solid dark blue) is plotted vs the final coordinate on a logarithmic scale, a long time ($t = 855\,568$) after the interaction with the barrier is over. The nominal locations of the maxima of the transmitted x_i [Eq. (8)] and reflected wave packets $-x_i$ are shown as the vertical dashed (cyan), dotted (green) and dashed-dotted (red) lines for the slow," intermediate, and fast wave packets, respectively. The solid magenta vertical line shows the location of the "screen" $x = x_M \equiv 40\,000$ [a.u.] where we measure the time distribution shown in Fig. 4.

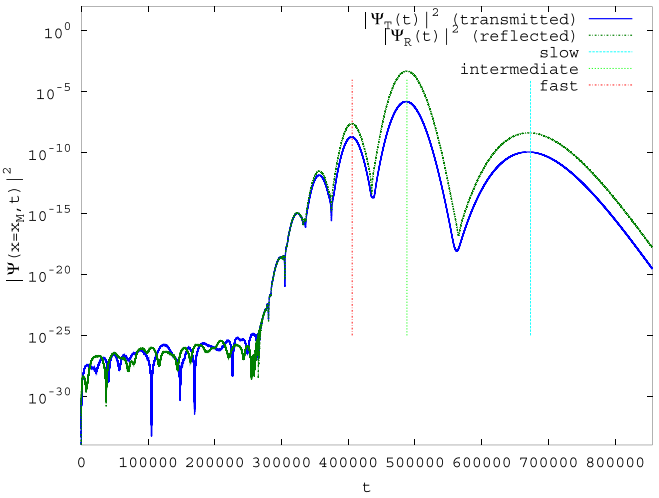

FIG. 4. The time dependence of the transmitted (solid blue line) and reflected (dashed-dotted dark green line which lies above the transmitted density line for $t \gtrsim 3 \times 10^5$ [a.u.]) densities $|\Psi(t)|^2$ as the wave packets cross the screen location x_M, are plotted on a logarithmic scale vs the time of arrival at the screen. The nominal arrival times for the wave packets t_i [see Eq. (9)] are shown as the vertical dashed (cyan), dotted (green), and dashed-dotted (red) lines for the slow, intermediate, and fast wave packets, respectively. Note that the subpackets are also well separated in the time domain.

III. TUNNELING FLIGHT TIME FOR THE BÜTTIKER-LANDAUER MODEL

The tunneling flight time for each of the scattered wave packets will be elucidated using a double pronged analysis:

(1) The first is to compare the transmitted wave packet flight time with the reflected wave-packet flight time. Any difference between them would be a reflection of a tunneling flight time.

(2) The second is to compare the transmitted wave-packet flight time in the presence of the barrier, with the same flight time for a wave packet scattered without the static barrier but with the oscillating one, that is, setting $V_0 = 0$ while keeping the value of V_1.

As is well understood, tunneling induces a momentum filtering effect when scattering a wave packet which has different momentum components [21]. The exponential dependence of the transmission probability on the initial momentum leads to a preference for transmission at the higher-momentum components of the incident wave packet. This filtering of the transmitted density, shortening the flight time of the transmitted particle masks the tunneling contribution to the flight time. To expose the tunneling time we consider the dependence of the flight times on the momentum width $\hbar^2\Gamma$. As Γ decreases, the momentum width of the incident wave packet is reduced and so also the momentum filtering effect, which vanishes in the limit that $\Gamma \to 0$.

A. Comparison of transmitted and reflected flight times

The momentum densities shown in Fig. 2 are also separable in the spatial domain, at a large distance from the barrier after the collision is over. Figure 3 shows the spatial density $|\Psi(x)|^2$ at the time $t = 855\,568$ by which the scattering event has ended. The nominal locations x_i of the three transmitted wave packets is estimated from the free particle dynamics as consisting of two contributions: one is the free particle motion with momentum p_0 from the initial mean location of the wave packet until reaching the barrier, and the other is the motion in the transmitted region with mean momentum $p_i = (p_-, p_0, p_+)$:

$$x_i = \frac{p_i}{M}\left(t + \frac{Mx_0}{p_0}\right), \tag{8}$$

These three locations are shown in Fig. 3 as the vertical (dashed cyan, dotted green, and dashed-dotted red) lines. Similarly, the centers of the reflected wave packets are at the locations $-x_i$. Since the time is long $t = 855\,568$ the different components are spatially well separated. Their peaks are higher by 8 to 10 orders of magnitudes relative to their minima.

The time distributions of the transmitted and reflected densities at the "screen" locations $x_M \equiv \pm 40\,000$ [a.u.] are plotted in Fig. 4. The nominal arrival times of the wave packets (based on free motion), shown in the figure as the vertical lines are

$$t_i = -\frac{Mx_0}{p_0} + \frac{Mx_M}{p_i}, \tag{9}$$

where p_i are as before the momenta (p_-, p_0, and p_+) for the "slow," "intermediate," and "fast" wave packets.

As may be seen from Fig. 4, the different energy components of the scattered and reflected wave packets are well separated also in the time domain. This enables us to associate a mean flight time difference between the transmitted and

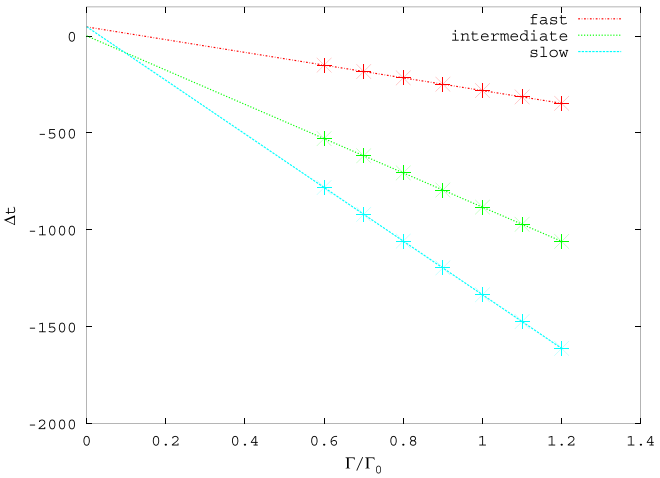

FIG. 5. The mean flight time differences Δt_i [Eq. (10)] between the various branches of the transmitted and reflected densities are plotted as a function of the width parameter Γ. The stars are the numerical values calculated from the time-dependent densities as in Eq. (10) and the lines are linear fits. The dashed (cyan), dotted (green), and dashed dotted (red) lines correspond to the slow, intermediate, and fast wave packets, respectively. The width parameter Γ_0 is the one given in Table I.

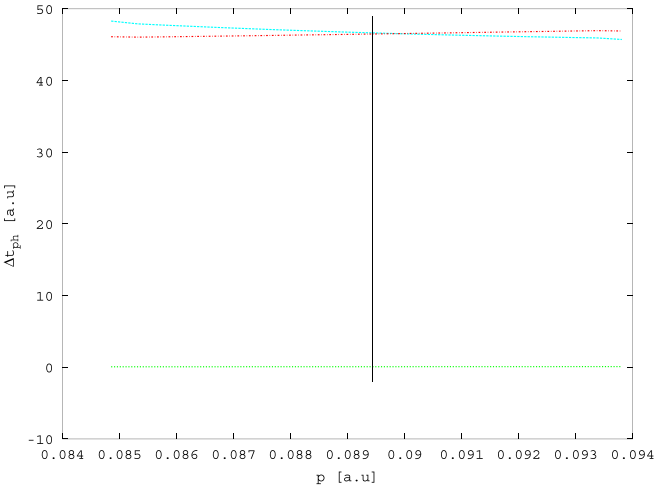

FIG. 6. The phase time differences between the transmitted and reflected waves are plotted for the three subpackets as a function of the initial scattering momentum p around the values of p_0 (vertical line) dashed (cyan), dotted (green), and dashed-dotted (red) for the slow, intermediate, and fast wave packets, respectively.

reflected wave packets calculated as

$$\Delta t_i = \frac{\int_{t_{\text{in}\,i}}^{t_{\text{fin}\,i}} dt\, t|\Psi_T(t)|^2}{\int_{t_{\text{in}\,i}}^{t_{\text{fin}\,i}} dt|\Psi_T(t)|^2} - \frac{\int_{t_{\text{in}\,i}}^{t_{\text{fin}\,i}} dt\, t|\Psi_R(t)|^2}{\int_{t_{\text{in}\,i}}^{t_{\text{fin}\,i}} dt|\Psi_R(t)|^2}, \tag{10}$$

where i is the index identifying the wave: slow, intermediate, and fast, $t_{\text{in}\,i}$, $t_{\text{fin}\,i}$ are the initial (start) and final (end) times for wave i, and Ψ_T, Ψ_R are the transmitted and reflected wave functions, respectively. For example, for the fast wave shown in Fig. 4, $t_{\text{in}} = 374\,054$ and $t_{\text{fin}} = 437\,405$ [a.u.].

The results for the Γ dependence of the mean flight time differences are shown in Fig. 5. There are a few notable aspects to these results. As expected, the momentum filtering effect shortens the transmitted mean times as compared with the reflected, that is why for finite Γ the mean time difference is negative. Second, all three plots are linear, as expected from the momentum filtering effect [11,19,20]. Most interestingly, though, are the mean time differences in the limit that $\Gamma \to 0$. These are found to be 47, 0.9, and 48.4 [a.u.] for the slow, intermediate, and fast waves, respectively. These turn out to be within the numerical accuracy of the linear fits to be the same as the phase time (differences) for the subpackets [23] as defined in the Appendixes by Eqs. (A9), (A10), and (B7). The momentum dependence of these phase times differences for the range of momenta covering the different branches of the scattered and reflected waves is shown in Fig. 6. The phase times at the nominal momentum p_0 are 46.65, 0.08, and 46.5 [a.u.] for the slow, intermediate, and fast waves, respectively. The excellent agreement between these phase time differences and the numerically computed mean time differences implies that the tunneling flight times are accounted for by the phase times.

B. Comparison of mean flight times with and without the static barrier

Naively, if one wants to determine the tunneling time all that is needed is to compute the mean transmission time through the barrier and compare it with the flight time of a free particle. However, this is not possible since, as already noted, the mean flight time of a free particle diverges due to the long time tail of the free particle density which goes as t^{-1}. This is why for many years one finds a comparison between the maxima of the transmitted densities in the presence of an interaction and without it. These comparisons have led to innumerable discussions concerning among others, group velocities [24,25], wave-packet shaping, and distortion [26] and wave-packet fronts [27,28]. One of the nice aspects of the Büttiker-Landauer model is that, without the static barrier, there remains a fluctuating barrier and this causes the long-time tail of the transmitted density to go as t^{-3} even without the presence of the static barrier [29], so that a "free particle" mean time is well defined. Moreover, in our computations the incident energy of the particle is much higher than the maximum fluctuation energy ($2V_1$) of the "free" particle, so that there is no tunneling through the "pure" fluctuating potential. This allows us to unravel the tunneling flight time by subtracting the mean-free particle flight time from the mean transmission flight time in the presence of both the static and fluctuating barrier.

The flight times of the transmitted wave packets in the presence of the barrier have been calculated [Eq. (10)] and shown (for Γ_0) in Fig. 4. The flight times in the absence of the barrier were also computed numerically by time evolution of the incident wave packet with the potential

$$V_F(x,t) = V_1 \sin(\omega t)\text{rect}\left(\frac{x}{2a}\right), \tag{11}$$

where V_1 is given in Table I. In the following we use the notation Ψ_F ("free") for the wave function propagated with the potential (11). The time evolution of Ψ_F is obtained with the

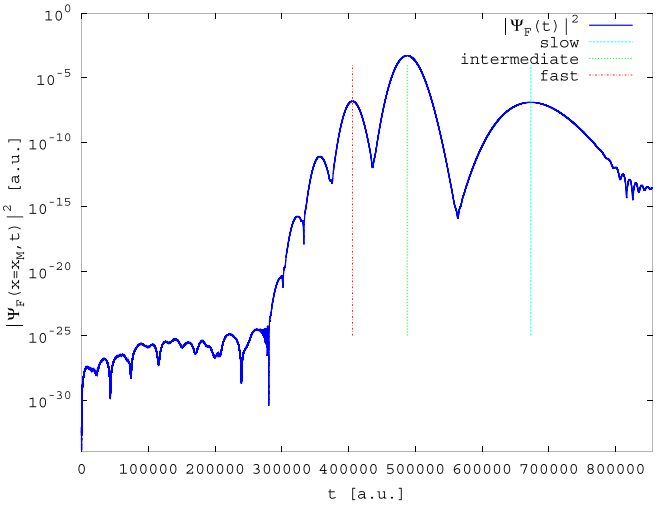

FIG. 7. The time dependence of the transmitted "free" density evolved using only the fluctuating part of the potential (solid blue line) at the spatial screen location x_M, is plotted using a logarithmic scale. The nominal arrival times for the transmitted wave packets t_i [see Eq. (9)] are shown by the vertical dashed (cyan), dotted (green) and dashed-dotted (red) lines for the slow, intermediate, and fast wave packets, respectively. Note that also in the absence of the static barrier, the different components of the scattered density are well separated in time.

same numerical procedure used for computing the time evolution with the static barrier. The resulting time dependence of the transmitted density of the free wave packet is plotted in Fig. 7 (for Γ_0) at the same spatial screen location x_M as for the wave packet with the static barrier. The main difference between the scattering with and without the static barrier is the much higher transmission probability in the latter case. The arrival time at the screen of the various components is (approximately) at the same expected flight times t_i as defined in Eq. (9).

The difference between the mean transmitted flight times with and without the static potential is calculated as

$$\Delta t_i = \frac{\int_{t_{\text{in}\,i}}^{t_{\text{fin}\,i}} dt\, t|\Psi_T(t)|^2}{\int_{t_{\text{in}\,i}}^{t_{\text{fin}\,i}} dt|\Psi_T(t)|^2} - \frac{\int_{t_{\text{in}\,i}}^{t_{\text{fin}\,i}} dt\, t|\Psi_F(t)|^2}{\int_{t_{\text{in}\,i}}^{t_{\text{fin}\,i}} dt|\Psi_F(t)|^2}, \qquad (12)$$

where, as before, i is the index identifying the wave: slow, intermediate, and fast $t_{\text{in}\,i}$ and $t_{\text{fin}\,i}$ are the initial (start) and final (end) times for wave i. The resulting mean flight time differences are plotted in Fig. 8 as a function of the (reduced) width parameter of the incident wave packet.

As when comparing the transmitted and reflected mean flight times, one finds a linear dependence on the width Γ, the negative slope is due to the momentum-filtering effect, which is much stronger in the presence of tunneling than without it. Most striking though is the fact that, in the limit $\Gamma \to 0$, the mean flight-time differences remain finite and are found to be -218.5, -196.8, and -75.16 [a.u.] for the slow, intermediate, and fast waves, respectively. The fact that these times are negative implies that the transmitted wave packet with the static barrier arrives at the "screen" location x_M *earlier* than the particle without the static barrier. This is a direct proof that tunneling reduces the mean flight time.

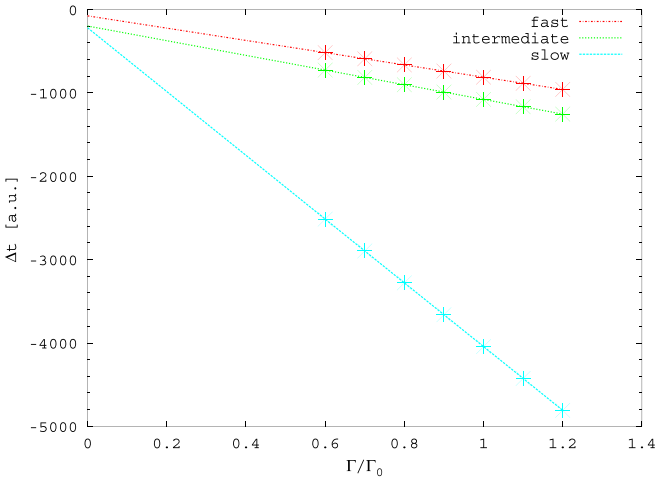

FIG. 8. The mean flight time differences Δt_i [Eq. (12)] between transmission with and without the static barrier are plotted as functions of the width parameter Γ. The stars are the values calculated from Eq. (12) and the continuous lines are linear fits. The dashed cyan, dotted (green), and dashed-dotted (red) lines are for the slow, intermediate, and fast wave packets, respectively. The value of Γ_0 is given in Table I.

Here too, this shortening of the tunneling flight time is well accounted for by the phase times. As before, these are calculated using Eqs. (B7) and (A9), once with the static barrier and once without. The phase time differences between the scattering with and without the static barrier are plotted in Fig. 9, and their values at the nominal momenta p_0 are -219.56, -197.54, and -76.18 [a.u.] for the slow, intermediate, and fast waves, respectively. They are in good agreement with the numerically determined mean flight time differences -218.5, -196.8, and -75.16 [a.u.], confirming that the mean

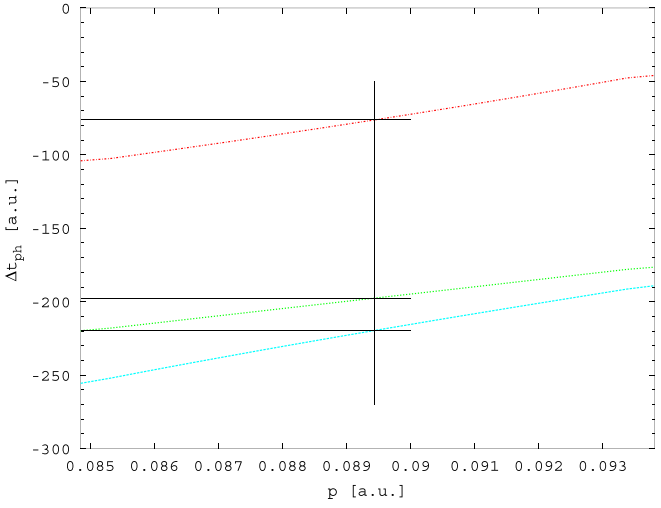

FIG. 9. The phase time differences for scattering with and without the static barrier for the three subpackets are plotted as functions of the initial momentum p around the values of p_0 (vertical line) dashed (cyan), dotted (green), and dashed-dotted (red) for the slow, intermediate, and fast wave packets, respectively. The horizontal lines show the values of the phase times differences at p_0.

tunneling flight time is the phase time. In comparison, the Büttiker-Landauer traversal time for tunneling is based on the central peak only and is defined as

$$t_{BL} = \frac{2aM}{\sqrt{2MV_0 - p_0^2}}. \tag{13}$$

For our conditions this gives a time of 447.21 which is evidently unrelated to the tunneling flight times discussed above. As is well understood, the Büttiker-Landauer traversal time is the semiclassical limit of the Pollak-Miller imaginary time defined as ($|T|^2$ is the relevant transmission probability)

$$t_{PM} = \frac{\hbar}{2|T|^2}\frac{d|T|^2}{dE}, \tag{14}$$

which may be evaluated separately for each of the three wave packets. One finds the imaginary times 486.72, 446.64, 562.42 for the slow, intermediate, and fast wave packets, respectively. These too are quite different from the phase times and so are not related to the flight times of the wave packets. It is noteworthy that the Pollak-Miller time for the intermediate wave packet is very close to the Büttiker-Landauer traversal time, which is its semiclassical estimate.

IV. DISCUSSION

The numerical computations presented in this paper lead to the unequivocal conclusion that in a time-of-flight experiment the tunneling contribution to the flight time is given by Wigner's phase time. The Büttiker-Landauer idea that such a time could be elucidated by employing an oscillating barrier served as an impetus to many researchers. The argument was simple and followed a similar one by Keldysh [30]. If the barrier oscillates rapidly with respect to the tunneling time, the particle will see the averaged static barrier. If it is very slow compared with the tunneling time, the transmission probability will be an average over the different barrier heights created through the slowly oscillating field. As argued by Büttiker and Landauer, the transition between the two regimes will occur when the tunneling time is $1/\omega$ (with ω the field frequency). Therefore, one could expect that a study of tunneling in the presence of an oscillating barrier would lead to elucidation of a tunneling time. Indeed, it does lead to a timescale—the imaginary "Pollak-Miller" time. But, as demonstrated in this paper, this imaginary time is not the tunneling flight time. The present computation shows that the flight time is given by the phase time, whether one has a fluctuating barrier or not. In this sense, the Büttiker-Landauer model does not shed any new light on the tunneling flight time.

This does not detract from the value of the Büttiker-Landauer experiment. The imaginary time depends on the interaction potential, in the semiclassical limit it is just (half) the period of the particle as it moves on the inverted potential at the energy $V - E$. Knowing this period reveals information on the barrier and its properties, which would be difficult to obtain otherwise. However, this time is not the tunneling flight time.

The idea of coupling the tunneling system to an external field in the interaction region also underlies the so-called Larmor time for tunneling [31,32]. Here, the scattered particle is assumed to have a spin and a weak field is present only in the region of the static barrier. This field causes a precession of the spin, the ratio of the shift in the spin angle to the magnetic field leads to identification of a Zeeman time which is then interpreted to be the tunneling time. This setup has been used in the recent experiments of Refs. [17,18]. The results presented in this paper suggest that the Larmor time, which is well defined, is also not the tunneling flight time which is given by the Wigner phase time. In the limit of a weak measurement, in which the measuring apparatus (the magnetic field) is only weakly coupled to the "system," the tunneling flight time will remain the phase time which does determine the tunneling flight time for the static isolated barrier.

One final comment is in order. Although the question what is the time it takes a particle to tunnel is stated simply, it is naive and in most cases not really answerable. Tunneling is not a quantum-mechanical concept. It is only due to our classical intuition which identifies regions in which motion is classically allowed or forbidden that we can define tunneling as motion in the classically forbidden region. For a square barrier, the region is well defined, but when scattering a wave packet, through a "smooth" barrier it is no longer possible to distinguish precisely between classically allowed and classically forbidden motion. The classically allowed region also affects the flight time. The only well-defined quantum question is how does the interaction potential affect the flight time. The present paper reaffirms that the general answer is through the phase time.

ACKNOWLEDGMENTS

We thank Prof. R. S. Dumont and Dr. T. Rivlin for stimulating discussions. This work was supported by a grant of the Israel Science Foundation.

APPENDIX A: TRANSMISSION AND REFLECTION COEFFICIENTS FOR THE BÜTTIKER-LANDAUER SYSTEM

The derivation of the transmission and reflection coefficients for the Büttiker-Landauer oscillating-barrier system have been given in some detail in Ref. [23], to leading order in the strength of the oscillating field V_1. Here, we generalize their results, without resort to perturbation theory, presenting them in a relatively simpler matrix form.

The dimension N of all the matrices and vectors will be odd and they are indexed from $-\frac{N-1}{2}$ to $\frac{N-1}{2}$ with the index corresponding to the value of n in Eq. (6). For example, for $N = 3$, the indices are -1, 0, and 1. We define the following diagonal $\mathbf{k}$ and $\boldsymbol{\kappa}$ matrices:

$$\mathbf{k} = \begin{pmatrix} \ddots & & & & \\ & k_{-1} & & & \\ & & k_0 & & \\ & & & k_1 & \\ & & & & \ddots \end{pmatrix},$$

$$\boldsymbol{\kappa} = \begin{pmatrix} \ddots & & & & \\ & \kappa_{-1} & & & \\ & & \kappa_0 & & \\ & & & \kappa_1 & \\ & & & & \ddots \end{pmatrix}. \tag{A1}$$

The incident wave vector contains only the k_0 element:

$$\mathbf{U} = \begin{pmatrix} 0 \\ \vdots \\ e^{-ik_0 a/2} \\ \vdots \\ 0 \end{pmatrix}. \tag{A2}$$

The Toeplitz matrix of Bessel functions is defined as

$$\mathbf{J} = \begin{pmatrix} J_0\left(\frac{V_1}{\hbar\omega}\right) & J_{-1}\left(\frac{V_1}{\hbar\omega}\right) & \dots & & \\ J_1\left(\frac{V_1}{\hbar\omega}\right) & J_0\left(\frac{V_1}{\hbar\omega}\right) & J_{-1}\left(\frac{V_1}{\hbar\omega}\right) & & \\ \vdots & J_1\left(\frac{V_1}{\hbar\omega}\right) & J_0\left(\frac{V_1}{\hbar\omega}\right) & \ddots & \vdots \\ & & \ddots & \ddots & J_{-1}\left(\frac{V_1}{\hbar\omega}\right) \\ & & \dots & J_1\left(\frac{V_1}{\hbar\omega}\right) & J_0\left(\frac{V_1}{\hbar\omega}\right) \end{pmatrix}. \tag{A3}$$

The continuity equations (see Appendix A of Ref. [23]) take the following form:

$$\mathbf{U} = -e^{i\mathbf{k}a/2}\mathbf{A} + \mathbf{J}[e^{-\boldsymbol{\kappa}a/2}\mathbf{B} + e^{\boldsymbol{\kappa}a/2}\mathbf{C}], \tag{A4}$$

$$i\mathbf{k}\mathbf{U} = i\mathbf{k}e^{i\mathbf{k}a/2}\mathbf{A} + \mathbf{J}\boldsymbol{\kappa}[e^{-\boldsymbol{\kappa}a/2}\mathbf{B} - e^{\boldsymbol{\kappa}a/2}\mathbf{C}], \tag{A5}$$

$$0 = -e^{i\mathbf{k}a/2}\mathbf{D} + \mathbf{J}[e^{\boldsymbol{\kappa}a/2}\mathbf{B} + e^{-\boldsymbol{\kappa}a/2}\mathbf{C}], \tag{A6}$$

$$0 = -i\mathbf{k}e^{i\mathbf{k}a/2}\mathbf{D} + \mathbf{J}\boldsymbol{\kappa}[e^{\boldsymbol{\kappa}a/2}\mathbf{B} - e^{-\boldsymbol{\kappa}a/2}\mathbf{C}]. \tag{A7}$$

The unknown vectors $\mathbf{A}$, $\mathbf{D}$ are the reflection and transmission coefficients and $\mathbf{B}$, $\mathbf{C}$ are the wave amplitudes inside the barrier. The exponents are N-dimensional vectors with the components $\exp(ik_j a)$, etc.

These equations may be solved formally analytically, using the following definitions:

$$\mathbf{p} \equiv i\mathbf{k}\mathbf{J} + \mathbf{J}\boldsymbol{\kappa}, \quad \mathbf{q} \equiv i\mathbf{k}\mathbf{J} - \mathbf{J}\boldsymbol{\kappa}, \tag{A8}$$

yielding for the transmission amplitudes:

$$\mathbf{D} = e^{-i\mathbf{k}a/2}\mathbf{k}^{-1}[\mathbf{p}\mathbf{q}^{-1} - \mathbf{q}\mathbf{p}^{-1}][\mathbf{p}e^{-\boldsymbol{\kappa}a}\mathbf{q}^{-1} - \mathbf{q}e^{\boldsymbol{\kappa}a}\mathbf{p}^{-1}]^{-1}\mathbf{k}\mathbf{U}, \tag{A9}$$

and for the reflection amplitudes:

$$\mathbf{A} = e^{-i\mathbf{k}a/2}\mathbf{k}^{-1}[\mathbf{q}e^{-\boldsymbol{\kappa}a}\mathbf{q}^{-1} - \mathbf{p}e^{\boldsymbol{\kappa}a}\mathbf{p}^{-1}] \times [\mathbf{p}e^{-\boldsymbol{\kappa}a}\mathbf{q}^{-1} - \mathbf{q}e^{\boldsymbol{\kappa}a}\mathbf{p}^{-1}]^{-1}\mathbf{k}\mathbf{U}. \tag{A10}$$

APPENDIX B: PHASE TIMES

Before interacting with the barrier, each spectral component of the incident coherent wave packet [Eq. (2)] evolves according to the free particle Hamiltonian $H(k) = \frac{p^2}{2M} = \frac{\hbar^2 k^2}{2M}$. The time evolved free wave packet is

$$\psi_{i,0}(x,t) = \left[\frac{\Gamma}{\pi}\right]^{1/4} \int dk \exp\left[-\frac{\Gamma}{2}(x - x_0)^2 + ikx\right] \times \exp\left(\frac{-i\hbar k^2 t}{2M}\right). \tag{B1}$$

The phase of this integral is $\Phi(k) = kx - \frac{\hbar k^2 t}{2M}$. The stationary phase requirement

$$\frac{d\Phi}{dk} = 0 \tag{B2}$$

results in $x - \hbar k t/M = 0$, specifying that each spectral element $p = \hbar k$ arrives at the location x at time $t = Mx/p$. This is correct for the free space propagation, but for the transmitted or reflected wave(s) one has to consider also the effect of the phase of the transmission or reflection coefficient on the stationary phase condition (B2). Let us express the transmission or reflection amplitude (written as X) as a function of k, by its magnitude and phase:

$$X(k) = |X(k)| \exp[i\varphi(k)]. \tag{B3}$$

The time-evolved transmitted or reflected wave packet becomes

$$\psi_{i,T/R}(x,t)\left[\frac{\Gamma}{\pi}\right]^{1/4} \int dk |X(k)| \times \exp\left[-\frac{\Gamma}{2}(x - x_0)^2 + ikx + i\varphi(k)\right] \exp\left(\frac{-i\hbar k^2 t}{2M}\right) \tag{B4}$$

and has a modified phase factor

$$\Phi(k) = kx - \frac{\hbar k^2 t}{2M} + \varphi(k). \tag{B5}$$

The stationary phase requirement (B2) now yields

$$t = \frac{Mx}{\hbar k} + \frac{M}{k}\frac{d\varphi}{dk} \equiv \frac{Mx}{\hbar k} + \Delta t_{ph} \tag{B6}$$

The additional (correction) term is called the *phase time*

$$\Delta t_{ph} = \frac{M}{k}\frac{d\varphi}{dk} \tag{B7}$$

and is used to compensate the effect of the transmission or reflection coefficient on the expected arrival time. One then associates a phase time with each transmission and reflection amplitude of the various ($n = -1, 0, 1$) branches created by the oscillating field.

[1] M. Büttiker and R. Landauer, Phys. Rev. Lett. **49**, 1739 (1982).
[2] E. Pollak and W. H. Miller, Phys. Rev. Lett. **53**, 115 (1984).
[3] E. Pollak, J. Chem. Phys. **83**, 1111 (1985).
[4] E. Wigner, Phys. Rev. **98**, 145 (1955).

[5] M. Büttiker, Phys. Rev. B **27**, 6178 (1983).
[6] S. Collins, D. Lowe, and J. Barker, J. Phys. C: Solid State Phys. **20**, 6213 (1987).
[7] A. M. Steinberg, Phys. Rev. Lett. **74**, 2405 (1995).
[8] T. E. Hartman, J. Appl. Phys. **33**, 3427 (1962).
[9] G. Nimtz, Prog. Quantum Electron. **27**, 417 (2003).
[10] R. S. Dumont, T. Rivlin, and E. Pollak, New J. Phys. **22**, 093060 (2020).
[11] T. Rivlin, E. Pollak, and R. S. Dumont, Phys. Rev. A **103**, 012225 (2021).
[12] M. Hentschel, R. Kienberger, C. Spielmann, G. A. Reider, N. Milosevic, T. Brabec, P. Corkum, U. Heinzmann, M. Drescher, and F. Krausz, Nature (London) **414**, 509 (2001).
[13] A. S. Landsman and U. Keller, Phys. Rep. **547**, 1 (2015).
[14] U. S. Sainadh, H. Xu, X. Wang, A. Atia-Tul-Noor, W. C. Wallace, N. Douguet, A. Bray, I. Ivanov, K. Bartschat, A. Kheifets, and R. T. Sang, Nature (London) **568**, 75 (2019).
[15] R. Dörner, V. Mergela, O. Jagutzki, L. Spielbergera, J. Ullrich, R. Moshammer, and H. Schmidt-Böckinga, Phys. Rep. **330**, 95 (2000).
[16] L. Torlina, F. Morales, J. Kaushal, I. Ivanov, A. Kheifets, A. Zielinski, A. Scrinzi, H. G. Muller, S. Sukiasyan, M. Ivanov, and O. Smirnova, Nat. Phys. **11**, 503 (2020).
[17] R. Ramos, D. Spierings, I. Racicot, and A. M. Steinberg, Nature (London) **583**, 529 (2019).
[18] D. C. Spierings and A. M. Steinberg, Proc. SPIE **11296**, 112960F-1 (2020).
[19] J. Petersen and E. Pollak, J. Phys. Chem. Lett. **8**, 4017 (2017).
[20] J. Petersen and E. Pollak, J. Phys. Chem. A **122**, 3563 (2018).
[21] Y. E. Lozovik and A. V. Filinov, J. Exp. Theor. Phys. **88**, 1026 (1999).
[22] R. Kosloff, J. Phys. Chem. **92**, 2087 (1988).
[23] K. Hara and I. Ohba, Phys. Rev. A **62**, 032104 (2000).
[24] R. U. Sexl and H. K. Urbantke, *Relativity, Groups, Particles* (Springer, Wien, New York, 2001).
[25] H. G. Winful, Phys. Rep. **436**, 1 (2006).
[26] G. Diener, Phys. Lett. A **223**, 327 (1996).
[27] R. Y. Chiao and A. M. Steinberg, Prog. Opt. **37**, 345 (1997).
[28] M. Büttiker and S. Washburn, Nature (London) **422**, 271 (2003).
[29] G. Muga, Top. Appl. Phys. **734**, 31 (2008).
[30] L. V. Keldysh, Sov. Phys. JETP **20**, 1307 (1965).
[31] A. I. Baz', Sov. J. Nucl. Phys. **4**, 182 (1967).
[32] V. F. Rybachenko, Sov. J. Nucl. Phys. **5**, 635 (1967).